Generalization of the deformation field method to simulate advanced reptation models in complex flows

Generalization of the deformation field method to simulate advanced reptation models in complex flow

E. A. J. F. Peters,[a] A. P. G. van Heel, M. A. Hulsen,

and B. H. A. A. van den Brule

J. M. Burgers Centre for Fluid Mechanics, Delft University of Technology, Rotterdamseweg 145, 2628 AL Delft, The Netherlands

(Received 2 December 1999; final revision received 22 March 2000)

Synopsis

In this paper we will show how the recently introduced deformation field method [Peters *et al*. (1999) and van Heel *et al*. (1999)] can be generalized to complex flow simulations of nontime–strain separable integral constitutive models. To illustrate this generalization we start with the time–strain separable Doi–Edwards model and we show how the approach can be generalized to nontime–strain separable models. As an example of such a model we consider the reptation model which was recently introduced by Mead *et al.* [Mead *et al*. (1998)]. In this reptation model also tube-stretch and convective constraint release are taken into account. We use both models to simulate startup of two-dimensional flow past a cylinder positioned between two parallel plates. © *2000 The Society of Rheology.* [S0148-6055(00)00804-X]

I. INTRODUCTION

In the last decades there has been considerable progress in understanding the mechanisms that play a role in polymer melt flow. The beginning of this progress was marked by the introduction of the reptation model by Doi and Edwards in 1978 [Doi and Edwards (1978a, 1978b, 1978c)]. In their approach Doi and Edwards modeled the topological constraints which are imposed on the test chain by the surrounding chains as a tube. By reptation, i.e., Brownian motion along its own contour, the test chain gradually escapes from its original confining tube. The predictions of the Doi–Edwards model for step–shear deformations are found to be in excellent agreement with experimental data. However, for steady shear flow the model predicts overly severe shear thinning, leading to a maximum in the shear stress as a function of shear rate. In spite of this latter discrepancy with experimental results, the concepts of a ''tube'' and ''reptation'' are of fundamental importance, and have served as the starting points for virtually all subsequent polymer melt theories.

One of the assumptions in the original Doi–Edwards model is that after deformation, the polymer chains instantaneously retract back to their equilibrium length, thus effectively removing chain stretching from the model. Marrucci and Grizutti (1988) and Pearson *et al*. (1989, 1991) relaxed this condition and introduced chain ex tensibility into the original reptation model by means of a finite retraction time. Indeed, calculations using the model of Pearson *et al*. do lead to improved predictions on startup of shear flow. For instance, in accordance with experiments the model predicts an overshoot of the first

[a]Author to whom correspondence should be addressed; electronic mail: e.a.j.f.peters@wbmt.tudelft.nl

normal stress difference, and it predicts that the strain at which this overshoot occurs increases with increasing shear rate. In spite of this improvement, however, in steady shear flows the Pearson model inherits the shear thinning behavior of the original Doi–Edwards model. This is because in steady-state shear flows, the polymers align in the flow direction. In this aligned orientation, the flow loses its grip on the polymers, and consequently the polymers retract back to their equilibrium length. Therefore, in the steady state shear regime, the Pearson model essentially reduces to the original Doi–Edwards description. As a consequence, the shear stress has a maximum as function of the shear rate.

In practice, however, it is found that the shear stress of polymer melts is nearly constant over a large range of shear rates. Therefore, another mechanism, which counteracts the above-mentioned alignment, must be included in the model. Marrucci (1996) has recently proposed such a mechanism, which he refers to as convective constraint release (CCR). The essential idea is that when the polymer chain deforms relative to its surrounding tube, i.e., when the overall deformation of the chain and its surroundings is not affine, geometric constraints are lost. This means that the chain can relax its orientation faster than when reorientation were caused by reptation only, so CCR suppresses the tendency of the polymers to align in the flow direction.

Based on the models of Pearson *et al*. (1989, 1991), Marrucci (1996), and Ianniruberto and Marrucci (1996), Mead *et al*. (1998) have formulated a microscopic model which combines both tube stretch and CCR. In this paper, we consider the so-called noncontour-variable reptation model introduced in Mead *et al*. (1998). In essence this model is a single segment model because coupling between different segments within one polymer chain is not taken into account.

In their paper, Mead *et al.* show how CCR affects both the relaxation of tube orientation and the relaxation of chain length. The resulting shear stress–shear rate curve turns out to have a local maximum, followed by a nearly constant but decreasing curve, which is followed by an increasing curve again. It has often been conjectured that such a nonmonotonic stress–shear-rate curve gives rise to flow instabilities and shear banding.

In this paper we focus on the flow behavior of the single-mode version of the Doi–Edwards model and the Mead–Larson–Doi model in a complex flow field; startup of flow past a cylinder positioned between two parallel plates. To this end we use the so-called deformation field method which was introduced for Rivlin–Sawyers models in Peters *et al*. (1999) and has been applied to the Doi–Edwards model in van Heel *et al*. (1999). In the present paper, we generalize this approach to include also tube-stretch and convective constraint release.

The paper is organized as follows: first we will discuss the single-mode Doi–Edwards model and the Mead–Larson–Doi model. Then we will briefly review the deformation field formulation, and we will show how tube stretch and CCR lead to the introduction of additional fields, viz. a stretch field and weight fields. A crucial ingredient in the deformation field formulation is the so-called partial orientation tensor. In this paper we compare two methods to calculate these partial orientation tensors. The first method is the subensemble method introduced in van Heel *et al*. (1999); the second method uses Currie's potential to approximate the orientation tensors. We compare the simulation results of the single-mode Doi–Edwards model and the Mead–Larson–Doi model for the flow past the cylinder. Our results are summarized in the conclusions.

II. GOVERNING EQUATIONS

The flow of an incompressible and isothermal fluid is governed by the continuity and momentum equations

$$\nabla \cdot \mathbf{v} = 0, \tag{1}$$

and

$$0 = -\nabla p + \nabla \cdot \boldsymbol{\tau}, \tag{2}$$

where we neglect inertial effects in the momentum balance, Eq. (2). In these equations, $\mathbf{v}$ is the velocity, p the pressure and $\boldsymbol{\tau}$ the extra-stress tensor. The latter generally consists of two contributions: a Newtonian contribution and a contribution due to the polymers

$$\boldsymbol{\tau} = \eta_s(\boldsymbol{\kappa} + \boldsymbol{\kappa}^T) + \boldsymbol{\tau}^p, \tag{3}$$

where η_s is the Newtonian (solvent) viscosity, $\boldsymbol{\kappa}$ is the transpose of the velocity–gradient tensor, $\boldsymbol{\kappa} = (\nabla \mathbf{v})^T$, and $\boldsymbol{\tau}^p$ is the polymer contribution to the extra stress.

III. SINGLE MODE DOI–EDWARDS MODEL

We consider a simplified version of the Doi–Edwards model, in which only the longest relaxation time of the original Doi–Edwards spectrum, the reptation time τ_d, is retained. In the rest of this paper we will employ the independent-alignment approximation (IAA). Similar to the exact Doi–Edwards model, the polymer stress $\boldsymbol{\tau}^p(t)$ is proportional to the orientation tensor $\mathbf{S}(t)$

$$\boldsymbol{\tau}^p(t) = 5G_0\mathbf{S}(t). \tag{4}$$

The constant G_0 is the elastic modulus, $G_0 = nk_BT$, where n is the number of tube segments per unit volume, k_B denotes Boltzmann's constant, and T denotes the absolute temperature. In passing we note that the numerical factor 5 in Eq. (4) reflects the above-mentioned assumption of the IAA. The orientation tensor $\mathbf{S}(t)$ is given by

$$\mathbf{S}(t) = \langle \mathbf{uu} \rangle(t), \tag{5}$$

where $\mathbf{u}$ is the momentary orientation of a tube segment, and the brackets denote ensemble averaging. The orientation tensor $\mathbf{S}(t)$ can equivalently be written as

$$\mathbf{S}(t) = \int_{-\infty}^{t} dt' \mu^{DE}(t;t')\mathbf{Q}(t;t'). \tag{6}$$

This expression shows that the total orientation tensor $\mathbf{S}(t)$ is a weighted average of *partial* orientation tensors $\mathbf{Q}(t;t')$. The tensor $\mathbf{Q}(t;t')$ is the present orientation tensor of those tube segments which were created at time t' in the past, which in the independent-alignment approximation is given by

$$\mathbf{Q}(t;t') = \langle \mathbf{u}(t)\mathbf{u}(t) \rangle_{t'}. \tag{7}$$

In this equation $\mathbf{u}(t)$ is the present orientation of a tube segment which was created at time t'. Since we focus our attention on tube segments which were created at time t', the brackets imply averaging *only over those tube segments which were created at* t' (this is underlined explicitly by the subscript t'). In the course of time, the relative contribution of a certain partial orientation tensor $\mathbf{Q}(t;t')$, labeled by its time of creation t', decreases, because due to reptation, the polymer chain gradually leaves its original confining tube. Therefore old partial orientation tensors contribute less to momentary orientation tensor $\mathbf{S}$ than partial orientation tensors corresponding to the tube segments which were recently created. To calculate the partial orientation tensor $\mathbf{Q}(t;t')$, we need the

present tube segment orientation $\mathbf{u}(t)$. This latter depends on its orientation at its moment of creation $\mathbf{u}(t')$ and on the subsequent deformation history, and is given by [Doi and Edwards (1986)]

$$\mathbf{u}(t) = \frac{\mathbf{F}(t;t')\cdot\mathbf{u}(t')}{|\mathbf{F}(t;t')\cdot\mathbf{u}(t')|}, \tag{8}$$

where $\mathbf{F}(t;t')$ is the deformation gradient tensor between t' and t. Substituting this in Eq. (7), we obtain

$$\mathbf{Q}(t;t') = \left\langle \frac{\mathbf{F}(t;t')\cdot\mathbf{u}(t')\mathbf{F}(t;t')\cdot\mathbf{u}(t')}{|\mathbf{F}(t;t')\cdot\mathbf{u}(t')|^2} \right\rangle_{t'}. \tag{9}$$

As was already pointed out above, Eq. (6) shows that the different partial orientation tensors $\mathbf{Q}(t;t')$ are not equally important in the integration, they are weighted by the factor $\mu^{DE}(t;t')dt'$. This factor is the fraction of tube segments present at time t which were created in the interval between $[t',t'+dt']$. Since we only take into account the mode with the longest relaxation time, the reptation time τ_d, the number of original tube segments created at t' shows a single exponential decay, hence

$$\frac{D}{Dt}\mu^{DE}(t;t') = -\frac{\mu^{DE}(t;t')}{\tau_d}. \tag{10}$$

In this equation the derivative on the left hand side is the material derivative, i.e., the right-hand side is evaluated at the position of a fluid particle while following this particle along its trajectory. Furthermore the weight factors are normalized such that their total probability adds to 1, i.e.,

$$\int_{-\infty}^{t} \mu^{DE}(t;t')dt' = 1, \tag{11}$$

thus

$$\mu^{DE}(t;t') = \frac{1}{\tau_d}\exp\frac{-(t-t')}{\tau_d}. \tag{12}$$

IV. MEAD–LARSON–DOI MODEL

Mead *et al.* have recently developed a reptation model which combines two mechanisms that had already been introduced in the literature separately, viz. tube-stretch and CCR. Here we will only briefly comment on their final equations, for a detailed discussion we refer the reader to the original paper [Mead *et al.* (1998)]. The polymer stress $\boldsymbol{\tau}^p$ is given by

$$\boldsymbol{\tau}^p(t) = 5G_0\lambda^2(t)\mathbf{S}(t). \tag{13}$$

This expression is very similar to the Doi–Edwards expression for the stress, Eq. (4), except for the factor $\lambda^2(t)$, which accounts for tube stretch. The *stretch parameter* λ is defined as the ratio of the actual length of the polymer to its length in absence of flow. The orientation tensor $\mathbf{S}(t)$ is still given by Eqs. (6) and (7), but the Doi–Edwards weight factor $\mu^{DE}(t;t')$ is now replaced by a weight factor $\mu(t;t')$. This weight factor is normalized to unity

$$\int_{-\infty}^{t} \mu(t;t')dt' = 1, \tag{14}$$

and obeys the following evolution equation

$$\frac{D}{Dt}\mu(t;t') = -\frac{\mu(t;t')}{\tau}. \tag{15}$$

Furthermore the relaxation time τ in Eq. (15) is the *total effective relaxation time* which, according to Mead *et al*., is given by

$$\frac{1}{\tau} = \frac{1}{\tau_d \lambda^2} + \frac{k}{\lambda}, \tag{16}$$

where

$$k = \boldsymbol{\kappa}:\mathbf{S} - \dot{\lambda}/\lambda. \tag{17}$$

In this equation $\dot{\lambda}$ denotes the material derivative of λ. The first term in Eq. (16) corresponds to relaxation by reptation only. The extra factor $1/\lambda^2$ was introduced by Mead *et al*. in order to make the model consistent with their so-called contour-variable model [Mead *et al*. (1998)]. The second term in Eq. (16) represents the extra relaxation of orientation due to CCR. When the test chain and its surroundings both deform affinely, the topological constraints on the test chain are not removed. Therefore, CCR can only occur when there are deviations from affine deformation of the test chain with respect to its surroundings. If the test polymer and its surroundings would deform affinely, then

$$\boldsymbol{\kappa}:\mathbf{S} - \dot{\lambda}/\lambda = 0, \tag{18}$$

and in that case the second term in Eq. (16) would vanish. Therefore the quantity k, as defined in Eq. (17), quantifies deviations from affine motion and can hence be seen as a measure for CCR.

Finally, the evolution equation for the stretch parameter λ is given by

$$\frac{D}{Dt}\lambda = \lambda\boldsymbol{\kappa}:\mathbf{S} - (\lambda - 1)/\tau_s - \frac{1}{2}k(\lambda - 1). \tag{19}$$

The first term on the right hand side of Eq. (19) corresponds to affine deformation. The second term corresponds to retraction of the polymer by the (linear) spring force; the time scale associated with this relaxation is the largest Rouse relaxation time of the polymer τ_s. The third term on the right hand side of Eq. (19) represents the relaxation of stretch due to CCR: when constraints are lost, the test polymer will tend to shrink.

The set of Eqs. (13)–(17) and Eq. (19) completely specify the dynamics of the Mead–Larson–Doi model.

In order to compare the Doi–Edwards model and the Mead–Larson–Doi model, we consider their behavior in stationary shear flow. In our calculations, following the paper of Mead *et al*. (1998), we fix the ratio of the reptation time τ_d and the Rouse time τ_s to 50

$$\tau_d/\tau_s = 50. \tag{20}$$

The curves shown in Fig. 1 were obtained using the deformation-field implementation (which is described in the following sections), and they are found to reproduce the results

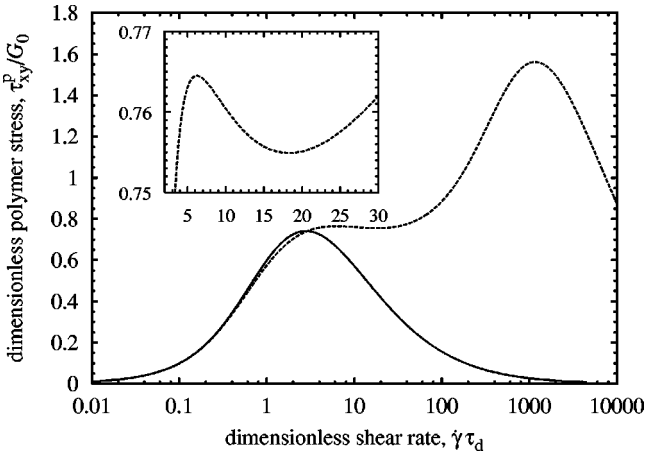

FIG. 1. Stress-shear rate curves for the Doi–Edwards model (solid line) and the Mead–Larson–Doi model (dotted line), both without added solvent viscosity. The ratio of the reptation time and the Rouse time is $\tau_d/\tau_s = 50$. The inset shows the local maximum in the Mead–Larson–Doi model.

of Mead *et al.* (1998), who calculated the curves in a different way. Note that the Doi–Edwards model has a shear-stress maximum, followed by excessive shear thinning. As was already mentioned above, this shear thinning is a consequence of the alignment of the polymers in the direction of the flow. The Mead–Larson–Doi reptation model leads to a completely different curve. Roughly speaking, there are three shear rate regimes: for shear rates $\dot{\gamma} < 1/\tau_d$, the Mead–Larson–Doi model is qualitatively the same as the Doi–Edwards model. For shear rates in the range $1/\tau_d < \dot{\gamma} < 1/\tau_s$, CCR will be dominant and the shear stress will remain more or less constant as a function of shear rate. From Fig. 1 we can see that the stress has a local maximum ($\tau_{xy} = 0.764G_0$) at a shear rate of $\dot{\gamma} = 6.2/\tau_d$. After this local maximum the stress remains nearly constant but *decreases* until a shear rate of $\dot{\gamma} = 18.5/\tau_d$, at which point the shear stress has a local minimum ($\tau_{xy} = 0.755G_0$). Finally, for shear rates $\dot{\gamma} > 1/\tau_s$, the flow is strong enough to stretch the polymers, leading to an increase in stress again. At very high shear rates, $\dot{\gamma} \approx 20/\tau_s$ (or $1000/\tau_d$), the stress decreases again and suffers extreme shear thinning. In this range, however, also higher Rouse relaxation modes, which are omitted in the Mead–Larson–Doi model, should be taken into account. Therefore, at these very high shear rates the model is no longer applicable.

V. DEFORMATION FIELDS

One of the key quantities in the models discussed above are the partial orientation tensors $\mathbf{Q}(t;t')$. In Sec. III these tensors were expressed in terms of the deformation gradient tensor $\mathbf{F}(t;t')$, but they can equivalently be written in terms of the Finger tensor $\mathbf{B}(t;t') = \mathbf{F}(t;t')\cdot\mathbf{F}^T(t;t')$

$$\mathbf{Q}(t;t') = \left\langle \frac{\mathbf{B}^{1/2}(t;t')\cdot\mathbf{u}(t')\mathbf{B}^{1/2}(t;t')\cdot\mathbf{u}(t')}{|\mathbf{B}^{1/2}(t;t')\cdot\mathbf{u}(t')|^2} \right\rangle_{t'}, \tag{21}$$

where $\mathbf{B}^{1/2}(t;t')$ denotes the square root of $\mathbf{B}(t;t')$. In constitutive equations the replacement of $\mathbf{F}(t;t')$ with $\mathbf{B}^{1/2}(t;t')$ is allowed whenever objectivity is obeyed. In this spe-

cific case, the legitimacy of the replacement can be checked more directly by noting that the initial distribution of orientations $\mathbf{u}(t')$ is isotropic. Therefore instead of applying $\mathbf{F}(t;t')$, $\mathbf{F}(t;t')\cdot R(t')$ will also give the same result for any history of rotations $\mathbf{R}(t')$.

Here we will profitably make use of the formulation of $\mathbf{Q}(t;t')$ in terms of the Finger tensor. Since we consider two-dimensional flow, both $\mathbf{F}(t;t')$ and $\mathbf{B}(t;t')$ have four components. By the incompressibility constraint the number of independent components can be reduced by one. However, $\mathbf{B}(t;t')$ is also symmetric, therefore it has only two independent components, one less than $\mathbf{F}(t;t')$. One can make several choices for these two independent variables; in this paper we use the method outlined in the appendix of Peters *et al*. (1999).

Since the initial tube segment orientations $\mathbf{u}(t')$ are fixed, the evolution of $\mathbf{Q}(t;t')$ is determined by the dynamics of the Finger tensor $\mathbf{B}(t;t')$. This latter satisfies the well-known evolution equation

$$\frac{D}{Dt}\mathbf{B}(t;t') = \boldsymbol{\kappa}(t)\cdot\mathbf{B}(t;t')+\mathbf{B}(t;t')\cdot\boldsymbol{\kappa}^T(t). \tag{22}$$

Again, the time derivative on the left-hand side is the material derivative, because we consider the deformation of a fluid particle while following this particle along its trajectory.

Both the partial orientation tensor and the Finger tensor can be defined at every point of the flow domain, so we can introduce tensor *fields* $\mathbf{Q}(\mathbf{x},t;t')$ and $\mathbf{B}(\mathbf{x},t;t')$, in which the spatial position is explicitly taken into account. The evolution equation for the Finger tensor field $\mathbf{B}(\mathbf{x},t;t')$ can be obtained from Eq. (22), noting that the latter equation is point-wise valid throughout the flow domain. Rewriting the material derivative, we obtain the evolution equation for $\mathbf{B}(\mathbf{x},t;t')$ in Eulerian form

$$\frac{\partial}{\partial t}\mathbf{B}(\mathbf{x},t;t')+\mathbf{v}(\mathbf{x},t)\cdot\nabla\mathbf{B}(\mathbf{x},t;t') = \boldsymbol{\kappa}(\mathbf{x},t)\cdot\mathbf{B}(\mathbf{x},t;t')+\mathbf{B}(\mathbf{x},t;t')\cdot\boldsymbol{\kappa}^T(\mathbf{x},t). \tag{23}$$

The initial condition for the Finger tensor field reads

$$\mathbf{B}(\mathbf{x},t';t') = \boldsymbol{\delta}, \tag{24}$$

where $\boldsymbol{\delta}$ denotes the unit tensor.

VI. WEIGHT FIELDS AND STRETCH FIELD

In Sec. V we introduced Finger tensor fields $\mathbf{B}(\mathbf{x},t;t')$. Of course the other quantities appearing in the Doi–Edwards model and in the model of Mead, Larson, and Doi can also be translated into *fields*, and the evolution equation for these fields can be obtained from the evolution equations of the associated quantities. This means that both models will give rise to *weight fields* $\mu(\mathbf{x},t;t')$, and that the Mead–Larson–Doi model will also lead to a *stretch field* $\lambda(\mathbf{x},t)$. The equations for these additional fields are easily obtained by making the corresponding original equations (those without the explicit $\mathbf{x}$ dependence) depend explicitly on position. The evolution equations for the weight fields follow from Eq. (15)

$$\frac{D}{Dt}\mu(\mathbf{x},t;t') = \frac{-\mu(\mathbf{x},t;t')}{\tau(\mathbf{x},t)}, \tag{25}$$

where $\tau(\mathbf{x},t)$ is the (total) relaxation time at position $\mathbf{x}$, at time t. As we have seen above, in the case of the Mead–Larson–Doi model $\tau(\mathbf{x},t)$ consists of two contributions, one due to reptation, and one due to convective constraint release. Therefore we factorize $\mu(\mathbf{x},t;t')$ as follows:

$$\mu(\mathbf{x},t;t') = \mu^{DE}(t;t')\mu^{\mathrm{CCR}}(\mathbf{x},t;t'). \tag{26}$$

Here the position-independent part $\mu^{DE}(t;t')$ corresponds to single-exponential decay by reptation only; the factor $\mu^{\mathrm{CCR}}(\mathbf{x},t;t')$ accounts for the decay due to convective constraint release. Substituting Eq. (26) into Eq. (25), and using Eq. (10) for μ^{DE} we obtain

$$\frac{D}{Dt}\mu^{\mathrm{CCR}}(\mathbf{x},t;t') = -\mu^{\mathrm{CCR}}(\mathbf{x},t;t')\left[\frac{1}{\tau(\mathbf{x},t)} - \frac{1}{\tau_d}\right]. \tag{27}$$

In this expression, the total relaxation time τ is given by Eq. (16).

The number of tube segments that is created in a certain time interval is exactly equal to the number of tube segments that disappears during this same interval. It is shown in the Appendix that

$$\mu(\mathbf{x},t';t') = \frac{1}{\tau(\mathbf{x},t')}. \tag{28}$$

Combining this result with Eqs. (12) and (26), we obtain

$$\mu^{\mathrm{CCR}}(\mathbf{x},t';t') = \frac{\tau_d}{\tau(\mathbf{x},t')}, \tag{29}$$

where $\tau(\mathbf{x},t')$ is the total relaxation time at position $\mathbf{x}$ at time t', and τ_d is the constant reptation time.

In the case of the original Doi–Edwards model, however, because $\mu^{DE}(t;t')$ is independent of spatial position, there is no need to introduce weight *fields*. This simplifies the simulations, because instead of calculating the evolution of a field throughout the domain, we only need to calculate the evolution in a single point. As was shown in van Heel *et al*. (1999), since $\mu^{DE}(t;t')$ is known analytically, we need not even monitor the weights in the course of the simulation, but we can calculate them before we start the simulation.

In the case of the Mead–Larson–Doi model, the field equation for the stretch parameter $\lambda(\mathbf{x},t)$ can be obtained from Eqs. (17) and (19). Substituting Eq. (17) into Eq. (19) and rearranging terms, we obtain

$$\frac{D}{Dt}\lambda(\mathbf{x},t) = \lambda(\mathbf{x},t)\boldsymbol{\kappa}(\mathbf{x},t):\mathbf{S}(\mathbf{x},t) - \frac{2}{\tau_s}\frac{\lambda(\mathbf{x},t)[\lambda(\mathbf{x},t)-1]}{\lambda(\mathbf{x},t)+1}. \tag{30}$$

In absence of flow the chain length is equal to the equilibrium length, and $\lambda = 1$. In this paper we assume that the fluid has been at rest until $t = 0$, so the initial condition for the stretch field reads

$$\lambda(\mathbf{x},0) = 1. \tag{31}$$

VII. SIMULATION ALGORITHM

In this section we will briefly discuss the implementation of the deformation field method. For a more detailed discussion we refer the reader to van Heel *et al*. (1999). In

the numerical implementation, the integral in the expression for the orientation tensor $\mathbf{S}(\mathbf{x},t)$ is replaced by a finite sum. Recall that $\mathbf{S}(\mathbf{x},t)$ is given by

$$\mathbf{S}(\mathbf{x},t) = \int_{-\infty}^{t} dt' \mu(\mathbf{x},t;t')\mathbf{Q}(\mathbf{x},t;t'). \tag{32}$$

In order to calculate the integral Eq. (32), we approximate the product $\mu(\mathbf{x},t;s)\mathbf{Q}(\mathbf{x},t;s)$, where s is a time in between two consecutive discrete times t'_k and t'_{k+1}, by linear interpolation. That is, we approximate the product $\mu(\mathbf{x},t;s)\mathbf{Q}(\mathbf{x},t;s)$ as follows:

$$\mathbf{Q}(\mathbf{x},t;s)\mu(\mathbf{x},t;s) = \sum_{k=0}^{\infty} \mathbf{Q}_k(\mathbf{x},t;t'_k)\mu^{DE}(t;t'_k)\mu^{\mathrm{CCR}}(\mathbf{x},t;t'_k)\phi_k(s). \tag{33}$$

In this expression, the base function ϕ_k is piecewise linear and nonzero only on the interval $[t'_{k-1},t'_{k+1}]$: $\phi_k(t'_{k-1}) = 0$, $\phi_k(t'_k) = 1$ and $\phi_k(t'_{k+1}) = 0$. In the simulations the intervals $[t'_{k-1},t'_{k+1}]$ on which the base functions are nonzero are not equidistant: they increase in size for increasing values of k. In this way we obtain a fine discretization of the integral, Eq. (32), in the region where the weight function μ changes rapidly (i.e., for $t' \approx t$), while we use a coarser discretization in the region where μ varies slowly. For a detailed discussion of this particular discretization, we refer the reader to the paper of Peters *et al.* (1999).

In the simulations we use N base functions $\phi_k(t'_k)$. Inserting the truncated approximation of Eq. (33) in Eq. (32) and performing the integration, we obtain

$$\mathbf{S}(\mathbf{x},t) = \sum_{k=0}^{N-1} W_k \mathbf{Q}_k(\mathbf{x},t;t'_k)\mu^{\mathrm{CCR}}(\mathbf{x},t;t'_k), \tag{34}$$

$$W_k = \int_{-\infty}^{t} dt' \mu^{DE}(t;t')\phi_k(t'). \tag{35}$$

These W_k can be interpreted as weights. Note that the weights W_k decrease when k increases, so it is natural to truncate the infinite summation. If there were no convective constraint release, i.e., if $\mu^{\mathrm{CCR}}(\mathbf{x},t;t'_k) = 1$, then the relative contribution of the partial orientation tensor $\mathbf{Q}(\mathbf{x},t;t')$ to the total orientation tensor $\mathbf{S}(\mathbf{x},t)$ would be W_k. Moreover, since the W_k are position independent, they can be calculated in advance of the simulation, and they have to be calculated only once. In the presence of CCR, however, the evolution of the additional weight fields $\mu^{\mathrm{CCR}}(\mathbf{x},t;t'_k)$ has to be taken into account through Eq. (27).

VIII. CALCULATION OF PARTIAL ORIENTATION TENSORS

As was already pointed out before, the partial orientation tensor $\mathbf{Q}(\mathbf{x},t;t')$ is a function of the Finger tensor $\mathbf{B}(\mathbf{x},t;t')$. Therefore, in the simulation we integrate the evolution equation of the Finger tensor fields. Subsequently we can calculate $\mathbf{Q}(\mathbf{x},t;t')$ as the average

$$\mathbf{Q}(\mathbf{x},t;t') = \left\langle \frac{\mathbf{B}^{1/2}(\mathbf{x},t;t')\cdot\mathbf{u}(t')\mathbf{B}^{1/2}(\mathbf{x},t;t')\cdot\mathbf{u}(t')}{|\mathbf{B}^{1/2}(\mathbf{x},t;t')\cdot\mathbf{u}(t')|^2} \right\rangle_{t'}. \tag{36}$$

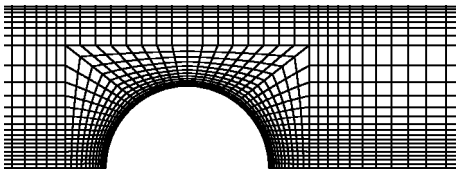

FIG. 2. Part of mesh M2. The total length of the periodic channel is 30 times the cylinder radius.

The brackets on the right-hand side denote an ensemble average over the unit vectors $\mathbf{u}(t')$, the end points of which at their moment of creation t' are distributed uniformly on the surface of the unit sphere. In van Heel *et al.* (1999), we introduced a method to calculate this ensemble average. In that approach we distribute M (typically 20–40) unit vectors $\mathbf{u}(t')$ on the surface of the unit sphere. In order to approximate a uniform distribution on the surface, the M vectors are *not* distributed randomly, but we distribute them such that they cover the sphere surface as homogeneously as possible. Subsequently we replace the integration in Eq. (36) by the average over these M vectors, i.e.,

$$\mathbf{Q}(\mathbf{x},t;t') \approx \frac{1}{M}\sum_{j=1}^{M} \mathbf{u}_j(\mathbf{x},t)\mathbf{u}_j(\mathbf{x},t), \tag{37}$$

where

$$\mathbf{u}_j(\mathbf{x},t) = \frac{\mathbf{B}^{1/2}(\mathbf{x},t;t')\cdot\mathbf{u}_j(t')}{|\mathbf{B}^{1/2}(\mathbf{x},t;t')\cdot\mathbf{u}_j(t')|}. \tag{38}$$

In principle this approach gives the exact value of $\mathbf{Q}(\mathbf{x},t;t')$ in the limit of large M, but from our simulations we found that a number of $M = 40$ unit vectors $\mathbf{u}_j(t')$, distributed as described above, is sufficient.

An alternative to the approach sketched above is to use Currie's approximation [Currie (1982)] which expresses $\mathbf{Q}(\mathbf{x},t;t')$ in terms of the Finger tensor $\mathbf{B}(\mathbf{x},t;t')$, its inverse and their invariants:

$$\mathbf{Q} = \frac{1}{(\mathrm{I}_B - 1 + 2\sqrt{\mathrm{II}_B + 13/4})}\left[\mathbf{B} - \frac{\mathbf{B}^{-1}}{\sqrt{\mathrm{II}_B + 13/4}}\right]. \tag{39}$$

In this expression I_B denotes the trace of $\mathbf{B}$ and II_B denotes the second invariant of $\mathbf{B}$,

$$\mathrm{II}_B = \tfrac{1}{2}(\mathrm{I}_B^2 - \mathrm{I}_{B^2}). \tag{40}$$

Since we assume incompressibility, II_B is equal to $\mathrm{I}_{B^{-1}}$, the trace of the inverse of $\mathbf{B}$. In our simulations we have used both the method using subensembles and Currie's approximation to calculate the orientation tensors $\mathbf{Q}(\mathbf{x},t;t')$. This allows us to compare Currie's approximation to the exact value of $\mathbf{Q}(\mathbf{x},t;t')$ in complex flows too.

IX. NUMERICAL METHODS

Our simulations are based on the finite element method. The mesh elements are quadrilaterals and the velocity and pressure are approximated by continuous biquadratic and discontinuous linear polynomials, respectively. In the deformation field method, apart from the velocity and pressure fields, we also have to calculate the time evolution of the Finger tensor fields $\mathbf{B}(\mathbf{x},t;t')$, and in the case of the Mead–Larson–Doi model also the

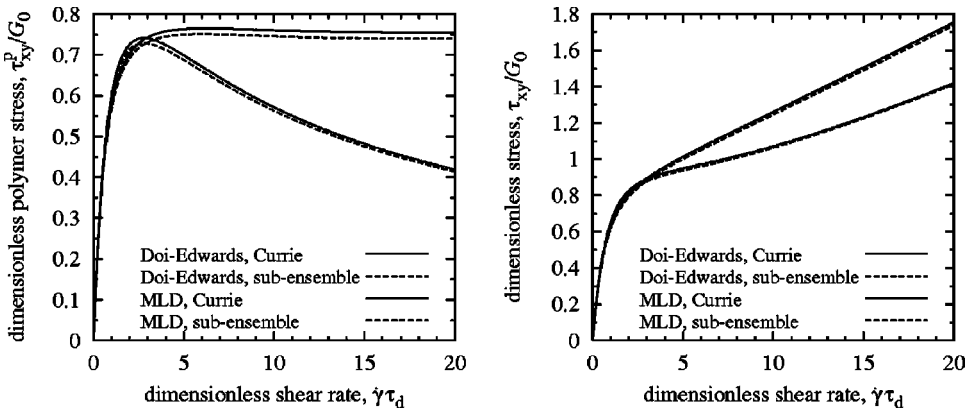

FIG. 3. The stress vs shear rate relations. The left graph shows the relation without extra Newtonian solvent viscosity. The right graph shows the changed relation when $0.05\,G_0\tau_d$ is added. Both the Doi–Edwards model and the Mead–Larson–Doi model have lost their excessive shear thinning behavior. The values obtained using the Currie approximation are only slightly higher than the exact values obtained by using the subensemble expression for the independent-alignment **Q** tensor (with subensemble size $M = 20$).

time evolution of the weight fields $\mu^{\mathrm{CCR}}(\mathbf{x},t;t')$ and of the stretch field $\lambda(\mathbf{x},t)$. These fields are treated by the discontinuous Galerkin method: they are approximated by bilinear polynomials which are discontinuous across the element boundaries. The discontinuous Galerkin implementation is particularly practical for the calculation of the convection terms in the evolution equations of the fields. In our simulations, we use a simple Euler forward discretization for the integration of the evolution equations of these fields. For instance, using a numerical time step Δt, the discretized version of Eq. (23) becomes

$$\begin{aligned}\mathbf{B}(\mathbf{x},t_{n+1};t') \;=\; & \mathbf{B}(\mathbf{x},t_n;t') - \mathbf{v}(\mathbf{x},t_n)\cdot\nabla\mathbf{B}(\mathbf{x},t_n;t')\Delta t \\ & + \Delta t[\boldsymbol{\kappa}(\mathbf{x},t_n)\cdot\mathbf{B}(\mathbf{x},t_n;t') + \mathbf{B}(\mathbf{x},t_n;t')\cdot\boldsymbol{\kappa}^T(\mathbf{x},t_n)] \qquad (41)\end{aligned}$$

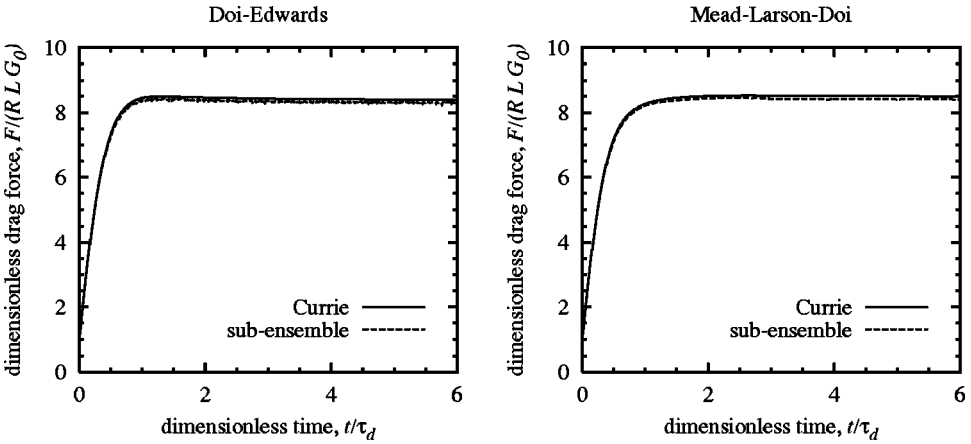

FIG. 4. Drag curves for the Doi–Edwards and the Mead–Larson–Doi model at We = 0.3.

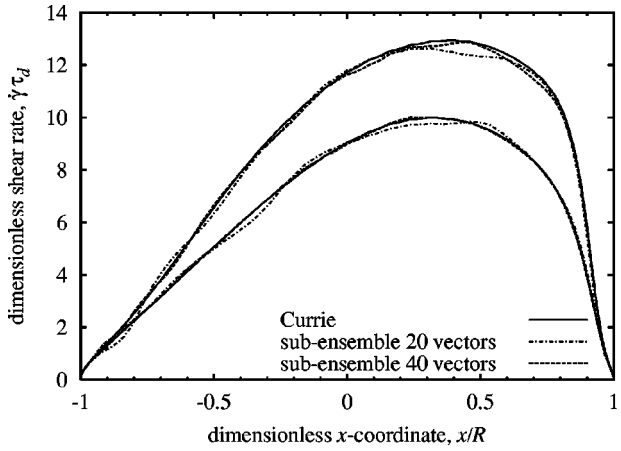

FIG. 5. Shear rate on the cylinder wall at We = 0.3 for both the Doi–Edwards model (upper curves) and the Mead–Larson–Doi model (lower curves). The subensembles consisting of 20 vectors show small wiggles. These wiggles are suppressed in simulations using ensembles of 40 vectors. There is almost no deviation between the Currie approximation and the subensemble calculation.

and similar equations for Eqs. (27) and (30). The continuity and momentum equations are solved using the so-called discrete elastic viscous stress split (DEVSS) method. For details concerning this particular implementation, we refer the reader to Hulsen *et al*. (1997).

X. RESULTS

To illustrate the use of the Mead–Larson–Doi model in a complex flow simulation, we use the ''cylinder in a channel'' geometry. This is a two-dimensional geometry. The width of the channel is twice the diameter of the cylinder and the cylinder is placed on the centerline. Periodic boundary conditions are used to connect the inlet and the outlet of the channel for all quantities except the pressure, which is periodic up to a linear func-

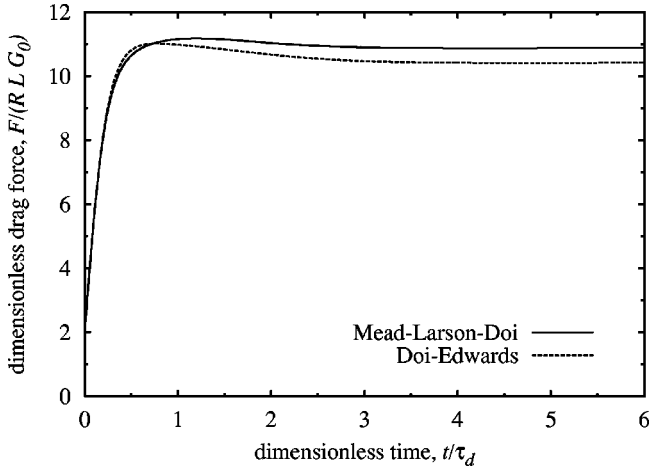

FIG. 6. Drag curves for the Doi–Edwards and the Mead–Larson–Doi model at We = 0.6 using the Currie potential.

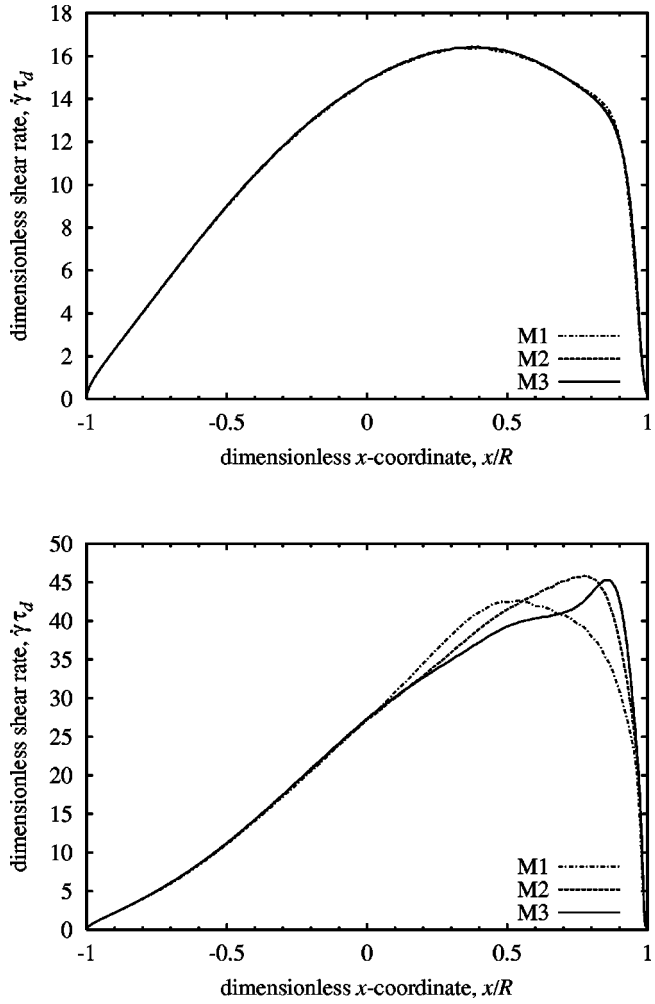

FIG. 7. Shear rate at the cylinder wall for the different meshes at We = 0.6. The upper graph shows the situation with $\eta_s = 0.05\, G_0 \tau_d$. The lower graph is the situation for $\eta_s = 0.005\, G_0 \tau_d$. No mesh convergence is reached in this last situation.

tion. By taking the total length of the channel to be 30 times the cylinder radius, the interaction of the cylinder with its mirror images is negligible.

Figure 2 shows the mesh that we use in the calculations (referred to as M2). At the cylinder wall the width of an element is $0.025R$, where R is the cylinder radius. At the channel wall, the width is $0.033R$. Mesh M2 consists of 2048 elements. For the purpose of investigating mesh convergence we use a coarser mesh (M1, coarsened by a factor 0.75 in all directions), and a finer mesh (M3, refined by a factor 1.25).

For all simulations presented in this paper a time step of $\Delta t = 0.001\, \tau_d$ is used. This is sufficient to simulate the reptation process accurately. The stretch time is a factor 50 smaller than the reptation time. This means it is 20 times larger than the discretization time step. In simulations of transient flows, using the Mead–Larson–Doi model, this will give rise to a small discretization error. In steady flow this error is absent. The reason is

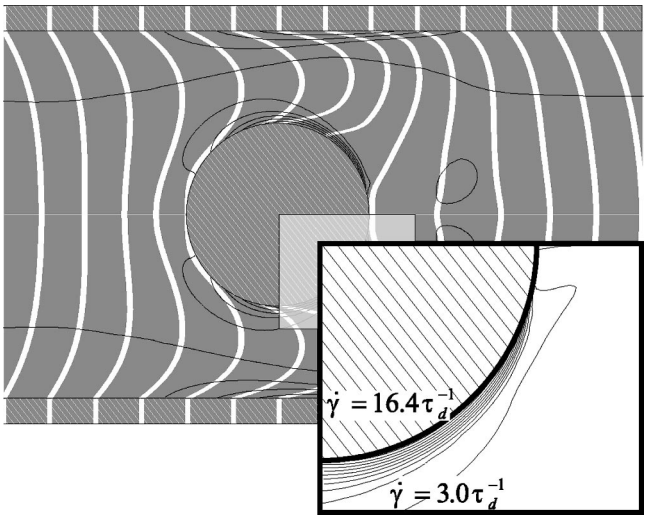

FIG. 8. Stationary flow for We = 0.6 with $\eta_s = 0.05\, G_0 \tau_d$. The black lines indicate vorticity contours. The white lines are profiles of the velocity in the stream wise direction.

that, in our implementation, the numerical method to solve the discretized stretch equation becomes independent of the time step for flows which are stationary in a Eulerian sense.

Since the effective relaxation time in the Mead–Larson–Doi model depends on the flow field we have to ensure that the numerical time step in the simulations is sufficiently small everywhere in the flow domain. For the Mead–Larson–Doi model this relaxation time has a minimal value of $0.058\,\tau_d$ in stationary shear flow (at $\dot{\gamma} = 750\,\tau_d^{-1}$). The highest shear rate in our simulations is $50\,\tau_d^{-1}$. For this stationary shear rate the relaxation time is $0.16\,\tau_d$. In transient situations the relaxation time can be smaller because segments are less well aligned (causing the term $\boldsymbol{\kappa}$:**S** to be larger). For $\dot{\gamma} = 50\,\tau_d^{-1}$ the

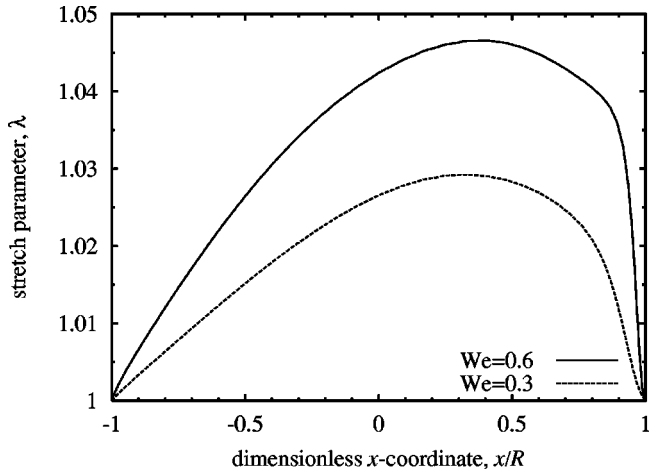

FIG. 9. The stretch parameter along the cylinder wall for We = 0.3 and We = 0.6.

shortest possible relaxation time is $0.09\,\tau_d$. The time step used in our simulations, $\Delta t = 0.001\tau_d$, is small enough to resolve all these time scales.

To characterize the flow we use the Weissenberg number based on the cylinder radius R, and the reptation time τ_d

$$\mathrm{We} = \frac{U\tau_d}{R}, \tag{42}$$

where U is the mean velocity in the channel.

Two sets of flow simulations are presented in this section. The first for We = 0.3 and the second for We = 0.6. For We = 0.3 we show the results of both the Doi–Edwards fluid and the Mead–Larson–Doi fluid. Second we compare a fully deterministic simulation using the Currie approximation, with a subensemble deformation field simulation, such as introduced in van Heel *et al*. (1999). For We = 0.6 some numerical issues like mesh convergence are also discussed.

A. Flow at We=0.3

Because of the excessive shear thinning behavior of the Doi–Edwards model, simulations beyond a certain Weissenberg number are unstable. The Mead–Larson–Doi model shows a shallow local stress maximum in the stationary stress versus shear-rate relation (see Fig. 3). Such a local maximum may lead to instabilities connected to multivaluedness of the solution [for examples of typical problems related to such a local maximum see Fyrillas *et al*. (1999) and Bishko *et al*. (1999)]. Only at extremely high shear rates, which are irrelevant for our simulations, does the model have a global maximum. Compared to the Doi–Edwards model the Mead–Larson–Doi model is less shear thinning. Nonetheless its behavior can still be characterized as very shear thinning. Even at We = 0.3, for the cylinder-in-a-channel geometry, this shear thinning gives rise to extremely thin boundary layers. These are thinnest on the cylinder wall in the downstream region. Using the meshes described above, the boundary layers cannot be fully resolved. Still finer meshes require more computer power (especially more memory) than is available to us.

The Weissenberg number of 0.3 is already quite low and decreasing it even further essentially masks the differences between the Doi–Edwards model and the model of Mead, Larson, and Doi. Another way to avoid extremely sharp boundary layers is to make the stress a monotonically increasing function of shear rate by the addition of extra Newtonian (solvent) viscosity. For the Mead–Larson–Doi model the addition of an extra solvent viscosity of $0.0015\,G_0\tau_d$ would have been sufficient to make the steady state stress monotonically increasing, whereas for the Doi–Edwards model we need to add a solvent viscosity of $0.03\,G_0\tau_d$ to achieve monotonicity. For these values of the added viscosity we still had convergence problems so we were forced to add significantly more. In all the simulations we present here we added a viscosity of $\eta_s = 0.05\,G_0\tau_d$ to both the Mead–Larson–Doi and the Doi–Edwards model (see Fig. 3). This increases the zero-shear-rate viscosity by 5%.

Figure 4 shows the drag force after startup of flow at a constant flow rate. The drag force is made dimensionless by means of elastic scaling, using as unit $G_0\,R\,L$, instead of the more common viscous scaling $(G_0\tau_d\,U\,L)$. Here L is the length of the cylinder, which is irrelevant because the problem is two dimensional. The left graph shows the response of the Doi–Edwards model. The upper curve is the result of the Currie approximation. The lower curve shows the subensemble deformation field result. The qualitative behavior is the same. There is a small difference in the numerical values at steady state

because of the small deviation of the Currie approximation from the exact (i.e., for infinite ensemble sizes) independent-alignment partial-orientation tensor **Q**. Curves generated using a subensemble size of 20 superimpose with those generated using a size of 40.

The right graph shows the results for the Mead–Larson–Doi model. The stationary drag is slightly higher for the Mead–Larson–Doi model than for the Doi–Edwards model. This is a consequence of the slight amount of tube stretching that occurs in the Mead–Larson–Doi simulation. The most apparent difference between the two models is the overshoot behavior. For the Doi–Edwards model there is an optimal orientation of the segments where the shear stress reaches its maximum. In sufficiently strong flows the orientation will pass this optimum when going from an isotropic state to a state where segments are much more aligned. Because the flow is very shear dominated the maximum in shear stress gives a maximum in the drag. In the Mead–Larson–Doi model the occurrence of the maximum is delayed and after the maximum is reached, the stress does not decrease that much anymore. The explanation is that, in this case, segments are reoriented due to the convective constraint release mechanism.

The subensemble computations and the computations using the Currie approximation agree very well. The subensemble solutions are wiggling around the results obtained using the Currie approximations. The initial distribution of vectors is chosen to be as isotropic as possible [van Heel *et al.* (1999)], but because of the finite ensemble size it is not fully isotropic. Ensembles at different places in the flow domain are rotated differently since they experience a different flow history. Therefore the deviation from isotropy in the initial distribution (which is independent of position), can cause small spatial variations at later times. It is shown in Fig. 5 that these wiggles are reduced when the initial distribution consists of 40 instead of 20 vectors. From Fig. 4 it appears that the wiggles have no significant influence on the drag.

B. Flow at We=0.6

At We = 0.6 the qualitative differences between the Doi–Edwards model and the Mead–Larson–Doi model are increased compared to the We = 0.3 situation. Figure 6 shows drag curves of two calculations using We = 0.6. Although the flow rate has increased by a factor of 2, the drag has not increased that much. Most of the increase of the drag is actually due to the viscous solvent contribution and not to the polymer contribution. For the Doi–Edwards model the difference between the value at the ''overshoot'' peak and the steady-state value has increased. Furthermore, the overshoot peak is reached earlier. The position of the peak scales with strain. This is fully consistent with the fact that the maximum in the drag force is related to an optimum in the segment orientation.

In order to show mesh convergence we investigate the behavior of the shear rate on the surface of the cylinder. Results for the different meshes M1, M2 and M3 are plotted in Fig. 7. The upper graph shows the situation with an added solvent viscosity of $0.05\,G_0\tau_d$. The results for the different meshes superimpose under mesh refinement. This is completely different for the second graph in Fig. 7. Here the solvent viscosity is reduced by a factor of 10 to $\eta_s = 0.005\,G_0\tau_d$, which is in fact still sufficient to remove

the stress maximum. The shear rates are now much higher and no mesh convergence is obtained. As discussed in the beginning of this section it is this failure to attain converged solutions which forced us to add a relatively high amount of solvent viscosity.

The steepness of the boundary layer at the cylinder wall, which is quite large even for the added $\eta_s = 0.05\, G_0 \tau_d$, is illustrated in Fig. 8. This plot shows the vorticity contour of the stationary flow for the We $= 0.6$ case. On a no-slip wall vorticity is equivalent to the shear rate. The contour lines shown in the figure are separated by an amount of approximately $1.5\tau_d^{-1}$. Not only large velocity gradients, but also large changes in velocity gradient are present near the cylinder wall. This steepness increases dramatically when less solvent viscosity is added.

Figure 9 compares the stretch parameter for We $= 0.3$ and We $= 0.6$ on the cylinder wall, again using $\eta_s = 0.05\, G_0 \tau_d$ in both cases. Even for the We $= 0.6$ case the stretch is relatively small, only about 5%. At high shear rates the CCR mechanism gives rise to a stationary distribution of the orientation of tube segments. Deformation and reorientation due to CCR are in equilibrium. This means that, without stretch, the stress will saturate at a finite, maximum value. In the Mead–Larson–Doi model, stretch can provide extra stress. In our simulations, unfortunately this contribution is relatively small compared to the contribution of the extra solvent contribution. The total polymer shear stress is $0.8G_0$ (see Fig. 3 at $\dot{\gamma}\tau_d = 16$). This is equal to the contribution of the solvent $(0.05\, G_0 \tau_d \times 16\tau_d^{-1})$.

XI. CONCLUSIONS

To conclude this paper we will summarize its main points.

An efficient method to simulate a class of nontime–strain-separable integral equations was presented. The method is a generalization of the *deformation field* method for time–strain-separable Rivlin–Sawyers equations as introduced in two previous papers [Peters *et al*. (1999) and van Heel *et al*. (1999)].

Due to spatial dependencies in the rate of relaxation the contribution of a deformation field to the total stress does not depend on ''age'' only, but also on the deformation history. Because of that the weighting in the integral becomes position dependent. In the original method it was possible to use precalculated weights which are valid for a whole deformation field. Here we had to introduce position dependent weight fields.

In the reptation-like constitutive equations for polymer melts, the integral over the deformation history gives an expression for the mean orientation of tube segments. Additional equations for the relaxation time and, e.g., tube stretch may be given. A flow-dependent relaxation time allows for inclusion of effects like convective constraint release. Recently proposed models like the Mead–Larson–Doi model and the pom-pom model [McLeish and Larson (1998)] include these effects. The generalized *deformation field* approach is capable of a full treatment of such constitutive equations without introducing extra approximations (like making the constitutive equation a differential equation). In this paper we presented an implementation of the Mead–Larson–Doi model.

In simulating the Mead–Larson–Doi model we followed two approaches. The fully ''macroscopic'' approach using the Currie approximation for the orientation **Q** tensor and a subensemble approach, introduced in van Heel *et al.* (1999), to calculate this **Q** tensor by ensemble averaging. The deviation between the Currie approximation and the ''exact'' subensemble results is very small.

Using the Mead–Larson–Doi model we performed complex flow simulations of the ''cylinder in a channel'' problem at two Weissenberg numbers (We $= 0.3$ and We $= 0.6$). After introducing an additional solvent viscosity $(0.05\, G_0 \tau_d)$ mesh conver-

gence was observed. Unfortunately this high solvent viscosity somewhat masks the differences between the Doi–Edwards model and the Mead–Larson–Doi model, which occur mostly at high shear rates.

The question whether the Mead–Larson–Doi model gives meaningful results when using a smaller or even no extra solvent viscosity is unresolved. For simulations with less solvent viscosity added we could not obtain mesh convergence. The reason is that the Mead–Larson–Doi model is very shear thinning. This leads to very sharp boundary layers which require a very fine mesh to resolve. The deformation field method is quite memory intensive. With the finest possible mesh allowed by our computer resources no mesh convergence was reached for a solvent viscosity of $0.005\,G_0\tau_d$.

ACKNOWLEDGMENT

The authors want to thank Jay D. Schieber for his helpful and pleasant discussions and suggestions during his stay at our laboratory.

APPENDIX: INITIAL CONDITION FOR WEIGHT FIELDS

The initial condition for the weights, i.e., $\mu(t';t')$, can be derived from the normalization condition Eq. (14)

$$\int_{-\infty}^{t} \mu(t;t')dt' = 1, \tag{A1}$$

and its evolution equation Eq. (15)

$$\frac{\partial}{\partial t}\mu(t;t') = -\frac{\mu(t;t')}{\tau(t)}. \tag{A2}$$

Upon differentiation of Eq. (A1) we obtain

$$\mu(t;t)+\int_{-\infty}^{t}\frac{\partial\mu(t;t')}{\partial t}dt' = 0. \tag{A3}$$

Now we use Eq. (A2) to replace the partial derivative of μ in the integral, thus

$$\mu(t;t)-\int_{-\infty}^{t}\frac{\mu(t;t')}{\tau(t)}dt' = 0. \tag{A4}$$

Since $\tau(t)$ does not depend on t', it can be put in front of the integral, and subsequently making use of the normalization condition, Eq. (A1) again, we obtain

$$\mu(t;t) = \frac{1}{\tau(t)}. \tag{A5}$$

References

Bishko, G. B., O. G. Harlen, T. C. B. McLeish, and T. M. Nicholson, ''Numerical simulation of the transient flow of branched polymer melts through a planar contraction using the 'pom-pom' model,'' J. Non-Newtonian Fluid Mech. **82**, 255–273 (1999).

Currie, P. K., ''Constitutive equations for polymer melts predicted by the Doi–Edwards and Curtis-Bird kinetic theory models,'' J. Non-Newtonian Fluid Mech. **11**, 53–68 (1982).

Doi, M., and S. F. Edwards, ''Dynamics of concentrated polymer systems: Brownian motion in the equilibrium state,'' J. Chem. Soc., Faraday Trans. 2 **74**, 1789–1801 (1978a).

Doi, M., and S. F. Edwards, ''Dynamics of concentrated polymer systems: Molecular motion under flow,'' J. Chem. Soc., Faraday Trans. 2 **74**, 1802–1817 (1978b).

Doi, M., and S. F. Edwards, ''Dynamics of concentrated polymer systems: The constitutive equation,'' J. Chem. Soc., Faraday Trans. 2 **74**, 1818–1832 (1978c).

Doi, M. and S. F. Edwards, *The Theory of Polymer Dynamics* (Oxford University Press, New York, 1986)..

Fyrillas, M. M., G. C. Georgiou, and D. Vlassopoulos, ''Time-dependent plane Poiseuille flow of a Johnson-Segalman fluid,'' J. Non-Newtonian Fluid Mech. **82**, 105–123 (1999).

Hulsen, M. A., A. P. G. van Heel, and B. H. A. A. van den Brule, ''Simulation of viscoelastic flows using Brownian configuration fields,'' J. Non-Newtonian Fluid Mech. **70**, 79–101 (1997).

Ianniruberto, G., and G. Marrucci, ''On compatibility of the Cox–Merz rule with the model of Doi and Edwards,'' J. Non-Newtonian Fluid Mech. **65**, 241–246 (1996).

Marrucci, G., ''Dynamics of entanglements: A nonlinear model consistent with the Cox–Merz rule,'' J. Non-Newtonian Fluid Mech. **62**, 279–289 (1996).

Marrucci, G., and N. Grizzuti, ''Fast flows of concentrated polymers: predictions of the tube model on chain stretching,'' Gazz. Chim. Ital. **118**, 179–185 (1988).

McLeish, T. C. B., and R. G. Larson, ''Molecular constitutive equations for a class of branched polymers: The pom-pom polymer,'' J. Rheol. **42**, 81–109 (1998).

Mead, D. W., R. Larson, and M. Doi, ''A molecular theory for fast flows of entangled polymers,'' Macromolecules **31**, 7895–7914 (1998).

Pearson, D. S., A. D. Kiss, L. J. Fetters, and M. Doi, ''Flow-induced birefringence of concentrated polyisoprene solutions,'' J. Rheol. **33**, 517–535 (1989).

Pearson, D., E. Herbolzheimer, N. Grizzuti, and G. Marrucci, ''Transient behavior of entangled polymers at high shear rates,'' J. Polym. Sci., Part B: Polym. Phys. **29**, 1589–1597 (1991).

Peters, E. A. J. F., M. A. Hulsen, and B. H. A. A. van den Brule, ''Instationary Eulerian viscoelastic flow simulations using time separable Rivlin–Sawyers constitutive equations,'' J. Non-Newtonian Fluid Mech. **89**, 209–228 (2000).

van Heel, A. P. G., M. A. Hulsen, and B. H. A. A. van den Brule, ''Simulation of the Doi–Edwards model in complex flow,'' J. Rheol. **43**, 1239–1260 (1999).